Tropical Cloud Feedbacks Estimated from Observed Multidecadal Trends

EMILY K. VAN DE KOOT,[a] MICHAEL P. BYRNE,[b,a] AND TIM WOOLLINGS[a]

[a] *Atmospheric, Oceanic and Planetary Physics, University of Oxford, Oxford, United Kingdom*
[b] *School of Earth and Environmental Sciences, University of St. Andrews, St. Andrews, United Kingdom*

(Manuscript received 27 May 2024, in final form 2 February 2025, accepted 21 February 2025)

ABSTRACT: Tropical cloud feedbacks are an important source of uncertainty in estimates of climate sensitivity. The extent to which changes in atmospheric circulation contribute to these feedbacks remains an open question. Here, all-sky radiative flux observations and an atmospheric reanalysis are used to estimate tropical cloud feedbacks from multidecadal trends (1985–2020) in cloud radiative effect and surface temperature. We decompose the observed feedbacks into dynamic and nondynamic components to quantify the impact of circulation trends. Narrowing and strengthening of tropical ascent lead to substantial dynamic feedbacks on regional scales that are similar in magnitude to the nondynamic feedbacks. However, as previously shown for high- and low-resolution climate models, large dynamic feedbacks in different circulation regimes are connected by the atmospheric mass budget and approximately cancel when averaged across the tropics due to the quasi-linear relationship between cloud radiative effect and vertical velocity. This results in small dynamic contributions to the tropical-mean net, longwave, and shortwave feedbacks. We suggest that this result will hold in future and thus that isolating the nondynamic components associated with individual cloud types can provide important insights into the processes controlling the tropical-mean cloud feedback and its uncertainty. Additionally, we show that feedbacks estimated from multidecadal trends differ from those estimated from interannual variability. We demonstrate that, for dynamic feedbacks, this is because changes are controlled by different mechanisms and this leads to a differing spatial distribution of temperature sensitivity. Finally, we provide new estimates of the uncertain combined tropical anvil area and albedo feedback using both multidecadal trends and interannual variability.

KEYWORDS: Tropics; Atmospheric circulation; Cloud radiative effects; Feedback; Trends

1. Introduction

Cloud feedbacks are the largest sources of uncertainty in estimates of equilibrium climate sensitivity (Zelinka et al. 2020). Long-standing difficulties in modeling clouds, caused by the wide range of impactful processes and scales, have resulted in observational studies becoming an important line of evidence for estimating their feedbacks (Sherwood et al. 2020).

Observational cloud feedback estimates often rely on the CERES dataset (Loeb et al. 2018) for top-of-atmosphere (TOA) fluxes. However, data collection only began in 2000, so CERES-based feedback estimates have largely focused on intermonthly or interannual covariability between cloud radiative effect (CRE) and surface temperatures. In an early study of this kind, Dessler (2010) found a global-mean short-term feedback of $+0.50 \pm 0.75$ W m^{-2} K^{-1} and, in a follow-up paper, assessed that dataset choice led to variations of 0.2–0.3 W m^{-2} K^{-1} in this estimate (Dessler and Loeb 2013). More recent global studies have produced similar estimates (e.g., Chao et al. 2024), while estimates of the equivalent tropical-mean cloud feedback include -0.06 ± 0.73 W m^{-2} K^{-1} (Williams and Pierrehumbert 2017) and 0.23 ± 0.40 W m^{-2} K^{-1} (Raghuraman et al. 2024). Recently, Raghuraman et al. (2023) used CERES to estimate the global-mean cloud feedback based on trends (rather than variability) in CRE and surface temperature and found a global-mean feedback close to zero (0.20 ± 0.34 W m^{-2} K^{-1}).

In this study, we use all-sky TOA radiative fluxes from the Diagnosing Earth's Energy Pathways in the Climate System (DEEP-C) dataset (Liu and Allan 2022) which spans 1985–2020. Combining DEEP-C all-sky fluxes with clear-sky fluxes from the ERA5 atmospheric reanalysis (Hersbach et al. 2020) allows for estimation of cloud feedbacks from trends over a period almost double the length of the CERES observational period. Although several other long-term products such as ISCCP (Young et al. 2018) and Cloud_cci AVHRR-PM (Stengel et al. 2020) include TOA radiative fluxes, trends in those datasets are likely influenced by variations in the contributing array of satellites, satellite drift, and calibration changes (Norris and Evan 2015; Hollmann and Pinnock 2020). DEEP-C carefully combines CERES (Loeb et al. 2018) with the well-characterized and bias-corrected Earth Radiation Budget Experiment Satellite wide field of view (ERBS WFOV) dataset (Wielicki et al. 2002; Wong et al. 2006) and was originally created to estimate the global TOA radiative flux imbalance (Liu et al. 2015).

Interpretation of observational estimates of cloud feedbacks is hindered by the complexity of the climate system. It

Denotes content that is immediately available upon publication as open access.

Supplemental information related to this paper is available at the Journals Online website: https://doi.org/10.1175/JCLI-D-24-0264.s1.

Corresponding author: Emily K. Van de Koot, emily.vandekoot@physics.ox.ac.uk

DOI: 10.1175/JCLI-D-24-0264.1

is well known that trends in TOA fluxes are driven by a range of radiative forcings alongside CO_2 (notably anthropogenic aerosols) and also by internal variability. Additionally, TOA flux anomalies comprise both instantaneous and surface temperature–driven responses of the climate system to these forcings (Raghuraman et al. 2021). However, increased understanding of the drivers of cloud feedbacks over recent decades may help constrain future cloud feedbacks.

In this study, we focus on interactions between clouds and the large-scale atmospheric circulation, which remains a persistent source of uncertainty in cloud feedbacks (Bony et al. 2015; Byrne and Schneider 2018; Bloch-Johnson et al. 2024). Furthermore, we compare feedbacks estimated from trends versus variability to learn about the extent to which contributing processes are similar on the two time scales. To isolate the influence of the large-scale circulation, we decompose cloud feedbacks by vertical velocity regime following Bony et al. (2004). This method has previously been used to investigate the contribution of circulation changes to cloud feedbacks in the CMIP5 ensemble (Byrne and Schneider 2018) and in cloud-resolving models (Mackie and Byrne 2023) and to place observational constraints on dynamic cloud feedbacks from the CMIP6 ensemble (Hill et al. 2023).

Motivated by where the largest uncertainties in cloud feedbacks lie (Sherwood et al. 2020), we limit our analysis to the tropics. Understanding and quantifying the changes in clouds associated with deep convection is particularly important as these clouds strongly reflect incoming shortwave radiation while also having high, cold cloud tops that generate a local greenhouse effect. Small changes in the balance of these effects could result in sizeable changes in TOA fluxes. The associated feedbacks are often related to changes in cloud altitude, albedo, and area. Sherwood et al. (2020) cited changes in the area of tropical anvils as the most uncertain cloud feedback, but recent studies have shown this feedback is likely small (McKim et al. 2024) and highlighted the albedo feedback as potentially playing an important role (Sokol et al. 2024). Importantly, global climate models (GCMs) and cloud-resolving models are not considered trustworthy for simulating changes in anvil area and albedo because of the sensitivity of results to subgrid-scale convection, turbulence, and microphysics (Sherwood et al. 2020).

The remainder of the paper is structured as follows. We begin by introducing the data and methods used. We then present feedback estimates using observed trends in CRE and surface temperature, including the decomposition into dynamic and nondynamic components. Following this, we discuss some implications of these results, including a new estimate of the combined anvil area and albedo feedback, and conclude with a summary and discussion.

2. Data

Two sources of all-sky TOA radiative fluxes are used: DEEP-C v5.0 (Liu and Allan 2022) and the ERA5 reanalysis (Hersbach et al. 2020). DEEP-C combines two satellite datasets over the period January 1985–July 2020 to create a continuous time series of TOA fluxes. The reconstruction uses CERES v4.1 from March 2000 onward, adjusted so that the climatological outgoing longwave radiation and reflected shortwave radiation for the period July 2005–June 2015 are consistent with ocean heat uptake estimates derived from Argo data (Loeb et al. 2018). Prior to March 2000, radiative fluxes are reconstructed using the monthly mean seasonal cycle derived from CERES v4.1 and deseasonalized spatial anomalies from ERA5 (Allan et al. 2014). The TOA flux variability is then constrained to match ERBS WFOV (v3.0) TOA fluxes at $10° \times 10°$ resolution (Liu et al. 2020). ERBS WFOV TOA fluxes are obtained from a single instrument covering a near-global domain (Wielicki et al. 2002) and have been corrected for known instrument and orbit drifts (Wong et al. 2006). There are two gaps in the satellite time series: in 1993 due to battery failure and during 1999–2000 due to changeover from ERBS WFOV to CERES (Allan et al. 2014). The gaps are filled by interpolating radiative flux anomalies from ERA5 and the absolute values on both sides of the gaps are adjusted based on the ensemble mean from ten AMIP6 model simulations (Liu et al. 2020).

The clear-sky TOA fluxes used are from ERA5. CRE is calculated by taking the difference between the all-sky and clear-sky radiative fluxes and then adjusting for noncloud effects using radiative kernels (Shell et al. 2008). Observation-based radiative kernels from *CloudSat*/*CALIPSO* are used (Kramer et al. 2019). All other data used are from the ERA5 reanalysis, including surface ("skin") temperatures.

Monthly mean data from 30°S to 30°N are used, conservatively remapped to a standard $1° \times 1°$ grid. Following Williams and Pierrehumbert (2017), the years 1991–92 are excluded because of the strong aerosol forcing associated with the Pinatubo eruption.

The use of multiple all-sky TOA radiative flux datasets allows for evaluation of their agreement and provides a measure of uncertainty in our results. Note, however, that the datasets are not fully independent as ERA5 is used in the DEEP-C reconstruction process. Furthermore, although ERA5 does not explicitly use CERES data within its assimilation scheme, it is possible that there is some overlap, for example, in the radiances used. For brevity, we will refer to the case with all-sky data from DEEP-C as "DEEP-C" and the case with all-sky data from ERA5 as "ERA5," despite both cases using ERA5 clear-sky data.

3. Methods

a. *Decomposing cloud feedbacks into dynamic and nondynamic components*

1) Framework

A method introduced by Bony et al. (2004) is used to isolate the component of the cloud feedback driven by circulation changes. The vertical pressure velocity (hereafter "vertical velocity") at 500 hPa, ω, is used as a proxy for the large-scale circulation. Discretizing ω into dynamic regimes allows the circulation to be characterized by a normalized probability density function $P(\omega)$ describing the relative occurrence of

each vertical velocity regime. The tropical-mean CRE, denoted $\overline{\mathrm{CRE}}$, can then be written as

$$\overline{\mathrm{CRE}} = \int P(\omega)\mathrm{CRE}(\omega)d\omega \approx \sum_{\omega} P(\omega)\mathrm{CRE}(\omega), \quad (1)$$

where $\mathrm{CRE}(\omega)$ describes the tropics-wide relationship between CRE and ω. In this study, each dynamic regime covers an interval of 10 hPa day^{-1}.

Bony et al. (2004) used this decomposition to study the CRE response to a discrete change in the climate system from a base state to a perturbed state (denoted using the prime symbol). Assuming the perturbed state can be described using a Taylor expansion about the base state, the sensitivity of $\overline{\mathrm{CRE}}$ to a change in mean surface temperature $\overline{T}$ can be expressed as

$$\frac{d\overline{\mathrm{CRE}}}{d\overline{T}} \approx \sum_{\omega}\left\{\mathrm{CRE}(\omega)\frac{P'(\omega) - P(\omega)}{\overline{T}' - \overline{T}} + P(\omega)\frac{\mathrm{CRE}'(\omega) - \mathrm{CRE}(\omega)}{\overline{T}' - \overline{T}} + \frac{[P'(\omega) - P(\omega)][\mathrm{CRE}'(\omega) - \mathrm{CRE}(\omega)]}{\overline{T}' - \overline{T}}\right\}. \quad (2)$$

The first term on the right-hand side of the equation is the circulation-driven, or "dynamic," component of the cloud feedback, and the second term on the right-hand side of the equation is the "nondynamic" component. The final term on the right-hand side of the equation is a nonlinear component resulting from interactions between dynamic and nondynamic changes.

In this study, we estimate (kernel-adjusted) tropical cloud feedbacks using time series of monthly mean CRE and surface temperature over the DEEP-C period. For each calendar month, we consider individual instances of that month to be perturbations relative to the monthly climatology and assume that these perturbations can be described using a Taylor expansion about the monthly climatology. We then estimate feedbacks for each calendar month—using all instances of that month over the complete time period—before averaging over calendar months to estimate the annual mean feedback. This method can be written as

$$\frac{d\overline{\mathrm{CRE}}}{d\overline{T}} \approx \sum_{\omega}\left\langle \mathrm{CRE}_{\mathrm{clim}}(\omega, m)\frac{dP(\omega, m, y)}{d\overline{T}(m, y)} + P_{\mathrm{clim}}(\omega, m)\frac{d\mathrm{CRE}(\omega, m, y)}{d\overline{T}(m, y)} + \frac{dP(\omega, m, y)d\mathrm{CRE}(\omega, m, y)}{d\overline{T}(m, y)}\right\rangle, \quad (3)$$

where m and y denote the month and year, respectively; $P_{\mathrm{clim}}(\omega, m)$ and $\mathrm{CRE}_{\mathrm{clim}}(\omega, m)$ are the monthly climatologies; $P(\omega, m, y)$, $\mathrm{CRE}(\omega, m, y)$, and $\overline{T}(m, y)$ are the data for individual months within the time series; and $\langle\cdot\rangle$ denotes a weighted average over months. For each calendar month, $dP(\omega, m, y)/d\overline{T}(m, y)$, $d\mathrm{CRE}(\omega, m, y)/d\overline{T}(m, y)$, and $[d\mathrm{CRE}(\omega, m, y)dP(\omega, m, y)]/d\overline{T}(m, y)$ are calculated by linear regression over all years.

To estimate cloud feedbacks from trends in CRE and surface temperature, we rewrite

$$\frac{d}{d\overline{T}} = \frac{d}{dy}\left(\frac{d\overline{T}}{dy}\right)^{-1} \quad (4)$$

in (3). In other words, for each calendar month, we compute the multidecadal linear trends in, e.g., $P(\omega, m, y)$ and divide by the trends in $\overline{T}(m, y)$. To compare behaviors on long and short time scales, we also use (3) to calculate cloud feedbacks based on year-to-year covariability of CRE and surface temperature.

We are presented with a choice as to which change in surface temperature is used to define the cloud feedback (Feldl and Roe 2013). Here, we use the tropical-mean surface temperature because this allows circulation changes to be viewed as part of the adjustment of the tropical atmosphere to the temperature perturbation. Sometimes, the local surface temperature is considered to be the natural process-based choice but, because the flow of air between regions is by definition nonlocal, insight into the coupling between clouds and circulation is lost with this approach.

Note that in previous literature, the nondynamic component is typically referred to as the "thermodynamic" component. However, there are many influences on cloud behavior beyond ω and local surface temperature, as has been demonstrated by recent work on cloud-controlling factors (e.g., Klein et al. 2018; Datseris et al. 2022; Wall et al. 2022); thus, we use a more neutral term.

2) Estimating the components

We begin by constructing climatologies of the probability density function and CRE for each calendar month, denoted $P_{\mathrm{clim}}(\omega, m)$ and $\mathrm{CRE}_{\mathrm{clim}}(\omega, m)$, respectively. These are calculated using the mean vertical velocity and CRE at each gridpoint for each calendar month. Here and throughout, area-weighting is used to account for changes in grid size with latitude. Next, we calculate CRE anomalies as a function of vertical velocity for individual instances of each month, $d\mathrm{CRE}(\omega, m, y)$. To achieve this, we calculate anomalies relative to the monthly CRE climatologies at each gridpoint, $d\mathrm{CRE}(\mathrm{lat}, \mathrm{lon}, m, y)$. We then subtract the noncloud contribution to these anomalies, calculated using the *CloudSat*/*CALIPSO* radiative kernels combined with ERA5 atmospheric variables. Finally, we combine the kernel-adjusted anomalies with $\omega(\mathrm{lat}, \mathrm{lon}, m, y)$ to find $d\mathrm{CRE}(\omega, m, y)$. To obtain $dP(\omega, m, y)$, we calculate $P(\omega, m, y)$ from monthly mean vertical velocities at each gridpoint and then calculate anomalies relative to the relevant monthly climatology, $P_{\mathrm{clim}}(\omega, m)$. The tropical-mean surface temperature anomalies for each month, $d\overline{T}(m, y)$, are the anomalies at each time step relative to the monthly climatology, $\overline{T}_{\mathrm{clim}}(m)$.

To estimate the trends in $dP(\omega, m, y)$, $d\mathrm{CRE}(\omega, m, y)$ for each calendar month, we linearly regress anomalies against years for each vertical velocity regime individually using the ordinary least squares method. Similarly, $d\overline{T}(m, y)/dy$ is calculated by regressing the tropical-mean surface temperature anomalies against years for each month. Note that by performing the regressions for each calendar month individually, we remove the influence of the seasonal cycle. Performing regressions over the full deseasonalized time series instead does not qualitatively affect the results.

To estimate $dP(\omega, m, y)/d\overline{T}(m, y)$, $d\text{CRE}(\omega, m, y)/d\overline{T}(m, y)$, and $[d\text{CRE}(\omega, m, y)dP(\omega, m, y)]/d\overline{T}(m, y)$ from year-to-year variability, $dP(\omega, m, y)$, $d\text{CRE}(\omega, m, y)$ and $dP(\omega, m, y)$ $d\text{CRE}(\omega, m, y)$ are regressed directly against $d\overline{T}(m, y)$ for each month. Additionally, for all variables, the monthly linear trend is removed prior to regression. For $d\text{CRE}(\omega, m, y)$, the trend is removed at each gridpoint, and for $dP(\omega, m, y)$, the trend is removed within each vertical velocity regime.

When presenting our results, we average over all calendar months and quote the feedback components and their constituent quantities in annual mean form. We rewrite the constituent quantities as follows: $\langle \text{CRE}_{\text{clim}}(\omega, m)\rangle = \text{CRE}(\omega)$, $\langle P_{\text{clim}}(\omega, m)\rangle = P(\omega)$, $\langle d\text{CRE}(\omega, m, y)/d\overline{T}(m, y)\rangle = d\text{CRE}(\omega)/d\overline{T}$, and $\langle dP(\omega, m, y)/d\overline{T}(m, y)\rangle = dP(\omega)/d\overline{T}$.

Errors are calculated for each vertical velocity regime. The errors on the monthly climatologies, $P_{\text{clim}}(\omega, m)$ and $\text{CRE}_{\text{clim}}(\omega, m)$, are taken to be the standard errors (σs) on the mean of $dP(\omega, m, y)$ and $d\text{CRE}(\omega, m, y)$ for that month, i.e., a measure of year-to-year variability. For the feedbacks calculated from trends, the errors on $dP(\omega, t)$, $y/d\overline{T}(m, y)$ and $d\text{CRE}(\omega, m, y)/d\overline{T}(m, y)$ are propagated from the standard errors on the slopes of the regressions of $P(\omega, m, y)$, $\text{CRE}(\omega, m, y)$, and $\overline{T}(m, y)$ against year. For the feedbacks calculated from variability, the errors on $dP(\omega, m, y)/d\overline{T}(m, y)$, $d\text{CRE}(\omega, m, y)/d\overline{T}(m, y)$ and $[dP(\omega, m, y)d\text{CRE}(\omega, m, y)]/d\overline{T}(m, y)$ are propagated from the standard errors on the slopes of the regressions of $dP(\omega, m, y)$, $d\text{CRE}(\omega, m, y)$, $dP(\omega, m, y)d\text{CRE}(\omega, m, y)$ and $d\overline{T}(m, y)$ against year. For the feedbacks calculated from variability, the errors on these terms are the standard errors on the slopes of the regressions of $dP(\omega, m, y)$, $d\text{CRE}(\omega, m, y)$, and $dP(\omega, m, y)d\text{CRE}(\omega, m, y)$ against $d\overline{T}(m, y)$. For DEEP-C, we additionally include an area-independent estimate of the standard error associated with instrument uncertainty which, based on calculations by Liu et al. (2020) and our own error propagation, we find to be 0.66 W m^{-2} K^{-1}. A more detailed discussion of this instrument error can be found in the online supplemental material. Errors on the dynamic, nondynamic, and nonlinear components, and on the annual mean forms of all terms, are calculated via error propagation.

For $d\text{CRE}(\omega, m, y)$ and $dP(\omega, m, y)d\text{CRE}(\omega, m, y)$, we require at least five values per vertical velocity regime to perform a regression. When this criterion is not fulfilled, the feedback is determined by linear interpolation of feedbacks from neighboring vertical velocity regimes. For $dP(\omega, m, y)$, months in which a vertical velocity regime is empty are included in the regression.

3) CAVEATS

The usefulness of the decomposition summarized by (3) lies in the insight it provides into the physical processes that control tropical cloud feedbacks. However, this framework does not represent all the ways in which circulation changes can influence cloud feedbacks. Clearly, the monthly mean vertical velocity at 500 hPa is an imperfect proxy for the full time-varying 3D tropical circulation and cloud feedbacks can be driven by circulation changes not associated with vertical motion at 500 hPa. But there are several more subtle caveats to applying the framework. First, the tropical-mean relationship between CRE and ω is not necessarily the same as the local relationship. Therefore, a change in the locations contributing to a particular vertical velocity regime can lead to a change in the mean CRE for that regime. In the decomposition, this effect will appear as a nondynamic feedback despite being driven by circulation shifts. A change in the locations contributing to a regime could result from, for example, a shift in the intertropical convergence zone (ITCZ). Second, circulation changes may impact clouds in other vertical velocity regimes via teleconnections mediated by variables other than ω. In this decomposition, this effect will also appear as a nondynamic feedback.

Although we refer to the cloud changes discussed here as feedbacks, we cannot assume that CO_2-induced temperature changes are the single cause of the cloud changes. Other factors such as different radiative forcings and the instantaneous response of the climate system to radiative forcings will also play a role. Furthermore, the observed trends cannot be assumed to be forced: internal variability may also contribute. Finally, we note that the use of monthly mean data may obscure the influence of submonthly variability (such as the Madden–Julian oscillation), so results could be different for daily data, for example.

b. *Mapping the spatial distribution of the decomposition components*

To better characterize the trend-derived dynamic and nondynamic feedback components, we map their spatial distributions. We begin by calculating the total cloud feedback at each gridpoint using the kernel-adjusted CRE anomalies and the tropical-mean surface temperature:

$$\text{Total feedback} = \left\langle \frac{d\text{CRE}(\text{lat}, \text{lon}, m, y)}{d\overline{T}(m, y)} \right\rangle. \tag{5}$$

Here, the derivative is calculated following (4): monthly CRE trends are calculated via linear regression at each gridpoint and divided by monthly trends in tropical-mean surface temperature before averaging over months. The error at each gridpoint is propagated from the standard errors on the CRE and temperature trends.

We then approximate the circulation-driven component of the feedback at each gridpoint. To do this, we create an artificial CRE dataset, denoted $\widehat{\text{CRE}}(\text{lat}, \text{lon}, m, y)$, in which the CRE is determined from $\omega(\text{lat}, \text{lon}, m, y)$ combined with the relevant $\text{CRE}_{\text{clim}}(\omega, m)$ curve. Then, at each gridpoint, we find $d\widehat{\text{CRE}}(\text{lat}, \text{lon}, m, y)$ by taking anomalies relative to the monthly climatology. The $d\widehat{\text{CRE}}(\text{lat}, \text{lon}, m, y)$ can be interpreted as the part of the CRE anomalies attributed solely to changes in vertical velocity. The dynamic component of the cloud feedback is then given as follows:

$$\text{Dynamic component} = \left\langle \frac{d\widehat{\text{CRE}}(\text{lat}, \text{lon}, m, y)}{d\overline{T}(m, y)} \right\rangle. \tag{6}$$

Finally, we can write as follows:

$$\text{Nondynamic component} = \left\langle \frac{d\text{CRE}(\text{lat}, \text{lon}, m, y)}{d\overline{T}(m, y)} - \frac{d\widehat{\text{CRE}}(\text{lat}, \text{lon}, m, y)}{d\overline{T}(m, y)} \right\rangle, \tag{7}$$

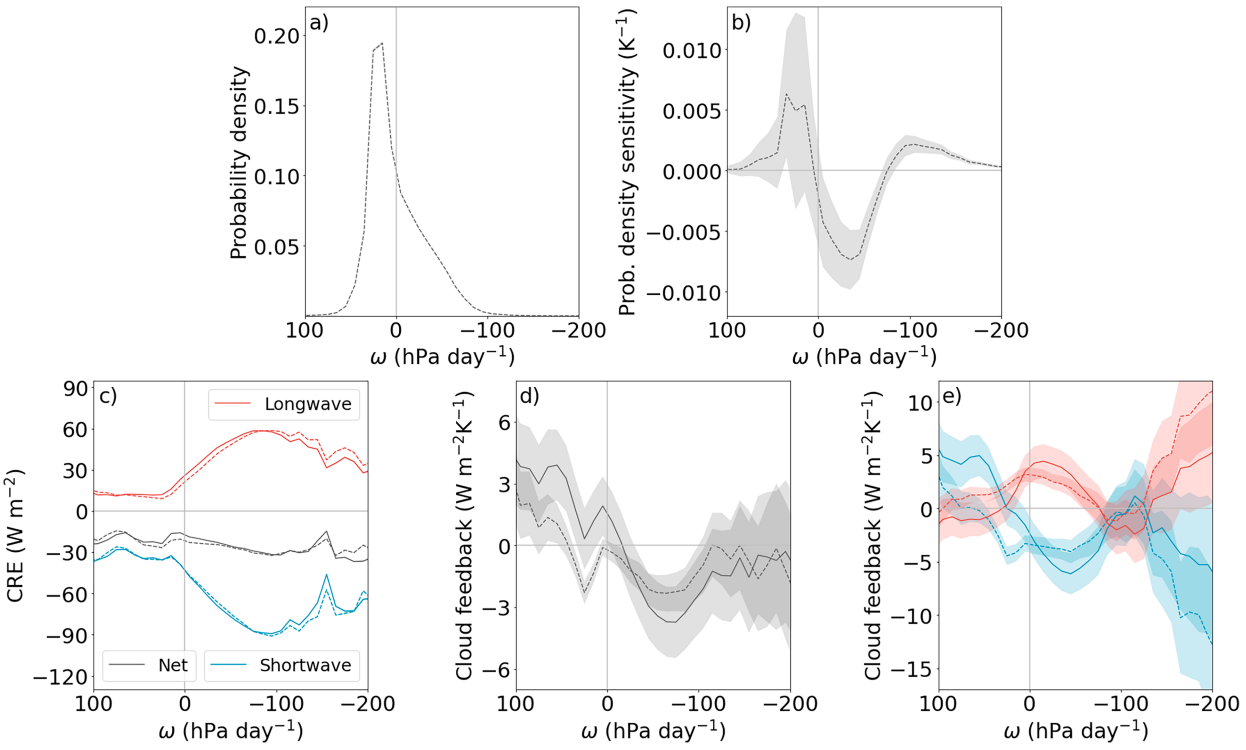

FIG. 1. DEEP-C (solid lines) and ERA5 (dashed lines) estimates of (a) the time-mean probability density $P(\omega)$, (b) the probability density sensitivity $dP(\omega)/d\overline{T}$, (c) the time-mean CRE(ω) distribution, and the (d) net and (e) longwave and shortwave cloud feedbacks $d\text{CRE}(\omega)/d\overline{T}$. Feedbacks are calculated from trends between 1985 and 2020 and climatologies are from the same period. Shading shows twice the standard errors.

assuming the nonlinear term is negligible. As for (5), the derivatives in (6) and (7) are calculated following (4).

Tropical-mean net, longwave, and shortwave feedback components calculated using (5)–(7) lie within twice the regression error of components calculated using (3) and (4) (not shown). However, this method is only intended to approximate the local feedback components. To focus on the large scales and to retain consistency with the tropics-wide decomposition above, we have chosen to use the tropics-wide $\text{CRE}_{\text{clim}}(\omega, m)$ monthly climatologies to calculate the dynamic component at each gridpoint. Therefore, the existence of a local nondynamic component could mean that the local relationship between CRE and ω is not captured by the tropical-mean relationship. Second, by calculating dynamic feedbacks for each gridpoint, rather than for each vertical velocity regime, we introduce a degree of spatial smoothing.

4. Results

To understand the drivers behind tropical cloud feedbacks estimated from observed multidecadal trends, we examine $P(\omega)$, CRE(ω), $dP(\omega)/d\overline{T}$, and $dCRE(\omega)/d\overline{T}$. We then consider how these terms combine to produce the dynamic and nondynamic feedback components which, in combination with the nonlinear feedback component, sum to give the total feedback.

a. *Circulation climatology and trends*

The time-mean probability distribution of vertical velocity regime occupancy $P(\omega)$ peaks sharply in regions of weak descent and is skewed, with faster vertical motion more common in ascending regions (Fig. 1a). Figure 1b shows $dP(\omega)/d\overline{T}$, the change in probability density with increasing tropical-mean surface temperature. With warming, there is a reduction in weak ascent frequency balanced by a combination of increased strong ascent frequency and a nonsignificant increase in descent frequency. This suggests a narrowing and strengthening of ascending regions across the tropics. The change in area covered by ascent is $-2.13\% \pm 0.70\%\ \text{K}^{-1}$ (or $-0.35\% \pm 0.11\%$ decade^{-1}). Here, and throughout the text, the errors quoted are twice the standard error unless otherwise specified. This exceeds the reduction found in other reanalysis datasets but agrees with observed trends based on outgoing longwave radiation, precipitation minus evaporation, and column relative humidity (Su et al. 2020). The increase in area covered by strong ascent ($\omega < -80$ hPa day^{-1}) is $1.70\% \pm 0.39\%\ \text{K}^{-1}$ (or $0.27\% \pm 0.06\%$ decade^{-1}). Reanalyses disagree on both the direction and magnitude of the trend in descending regions (see Fig. 3 of Su et al. 2020).

At a regional scale, the picture is more complex, with a clear contrast in behaviors over land and ocean. Figure 2 shows the local sensitivity of vertical velocity to tropical-mean warming. Over the central and east Pacific and the Atlantic, we see narrowing and strengthening of the ITCZ in agreement with previous studies (Wodzicki and Rapp 2016; Byrne et al. 2018). Despite more complex trends over the west Pacific and the Maritime Continent, we see some evidence of strengthening of the Walker cell. Ma and Zhou (2016) found strengthening of the zonal mass

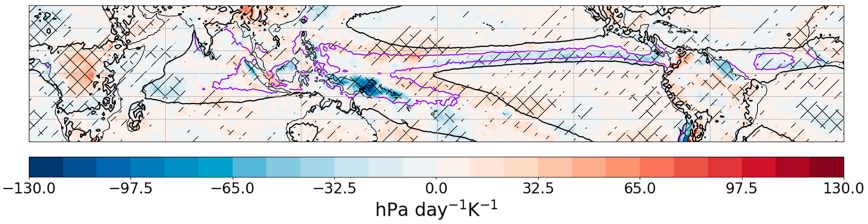

FIG. 2. Changes in vertical velocity per degree tropical warming calculated from trends between 1985 and 2020. Regions where the magnitude of the sensitivity to warming is larger than the standard error are hatched and regions where it is larger than twice the standard error are cross-hatched. The black contour divides regions of climatological ascent and descent. Note that in ascending regions, blue shading corresponds to strengthening ascent and red shading corresponds to weakening ascent, while in descending regions, red shading corresponds to strengthening descent and blue shading corresponds to weakening descent. The purple contour shows oceanic regions in which $\omega < -70$ hPa day^{-1} more than 15% of the time.

streamfunction over the Pacific between 5°N and 5°S across seven reanalyses. Considering Fig. 2, our results largely agree with this, although we see a large increase in ascent strength in the South Pacific convergence zone (SPCZ) and a decline in the west Pacific ITCZ. In descending regions, results are more clearly La Niña–like, with widespread strengthening of descent, strengthened easterlies at 850 hPa, and some evidence of strengthened westerlies at 200 hPa (Figs. 1 and 2 in the online supplemental material, respectively).

The trend toward narrowing and strengthening ascent is less evident over land, despite the land-only $dP(\omega)/d\overline{T}$ distribution showing similar behavior to the tropics-wide case (not shown). This suggests that the boundaries of the regions of climatological ascent do not necessarily narrow over land, rather we increasingly find smaller regions of stronger ascent with a more complex spatiotemporal distribution than over ocean. Alongside this, we find shifts in the location of ascent over land. There is a substantial reduction in ascent over central equatorial Africa, present in all seasons. Changes in ascent location are less clear over South America, but over both continents, we see a weakening of the westerlies at 200 hPa during JJA and SON (supplemental Fig. 2). The weakening is centered south of the climatological maximum suggesting a trend toward reduced northward progression of the ITCZ during boreal summer over both continents.

b. *CRE(ω) climatology and trends*

The climatological relationship between vertical velocity and the longwave, shortwave, and net CREs is shown in Fig. 1c. Interestingly, although the longwave and shortwave CREs exhibit substantial variation with vertical velocity, they combine to produce a relatively constant net CRE across vertical velocity regimes. In regions of strong descent ($\omega > 25$ hPa day^{-1}), the longwave and shortwave CREs do not vary with ω. In these regions, clouds are generally confined to low elevations, and this result suggests that their properties may be decoupled from vertical velocity at 500 hPa and instead determined by boundary layer processes. In regions of ascent and weak descent, we find increasing longwave and shortwave CRE magnitudes with increasing ω. Given that ω is the monthly mean ascent, its value is set not only by the strength of individual updrafts but also by their frequency. Thus, this positive relationship is likely associated with both increasing frequency and increasing strength of convection. We suggest that the increased frequency of convection leads to increased cloud fraction, while increased strength of convection leads to taller convective towers and thus increased cloud albedo (strengthening shortwave CRE) and decreased cloud-top temperature (strengthening longwave CRE). In regions of very strong ascent, the longwave and shortwave CREs no longer strengthen with increasing ω. There are a range of possible reasons for the nonlinear relationship between CRE and vertical velocity in ascending regions. One option is that less persistent updrafts (leading to a lower monthly mean ascent) may lead to stronger CRE than more consistent upward motion because high clouds can linger during downdrafts and, because the atmosphere is drier during these periods, there is greater contrast between clear- and cloudy-sky regions (Datseris et al. 2022). Another possibility is that, given stronger ascent is more spatially localized and more likely to occur over land than weaker ascent (not shown), the nonlinearity could reflect regional variability in the relationship between CRE and vertical velocity. For example, cloud formation over land may be inhibited by limited moisture availability.

Cloud feedbacks within individual vertical velocity regimes are shown in Figs. 1d and 1e. We find that, to first order, the slopes of the CRE(ω) relationships have steepened over the period 1985–2020, i.e., the tropics-wide coupling between clouds and circulation has strengthened. Considering the relationship between cloud feedback and vertical velocity more closely, we see significant strengthening of the longwave and shortwave CREs with increasing tropical-mean surface temperature in weakly descending and in ascending regions. There are two interesting nuances here: First, the variation of feedback strength with ω differs for the longwave and shortwave CREs in these regions (Fig. 1e). The longwave feedback is larger for 25 hPa day$^{-1} > \omega > -20$ hPa day^{-1} and the shortwave feedback is larger for -20 hPa day$^{-1} > \omega > -80$ hPa day^{-1}. Second, ERA5 and DEEP-C disagree on shortwave feedbacks in regions of weak descent, with ERA5 showing strong negative feedbacks. In regions of very strong ascent, we again find positive longwave and shortwave feedbacks, but they are not statistically significant. In regions of strong descent, longwave feedbacks are weak, and ERA5 and DEEP-C once again

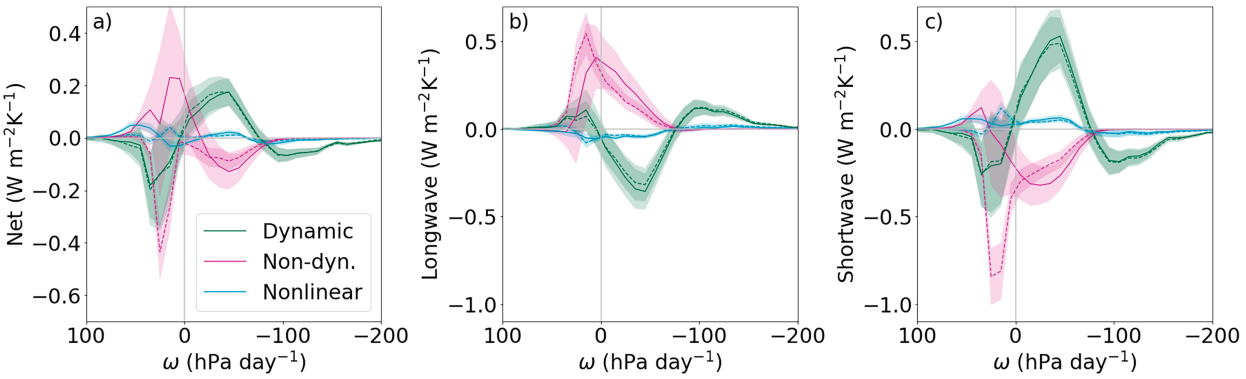

FIG. 3. DEEP-C (solid lines) and ERA5 (dashed lines) estimates of the contribution of each vertical velocity regime to the dynamic, nondynamic, and nonlinear components of the tropical-mean (a) net, (b) longwave, and (c) shortwave cloud feedbacks. Feedbacks are calculated from trends between 1985 and 2020 and are split into components following [(3)]. Shading shows twice the standard errors.

disagree on shortwave feedbacks, with DEEP-C showing a strong positive feedback and ERA5 showing no significant feedback. The drivers of these feedbacks will be discussed in more detail in section 4c.

c. *Dynamic and nondynamic components of the tropical-mean cloud feedback*

Figure 3 shows the contribution of each vertical velocity regime to the dynamic, nondynamic, and nonlinear components of the tropical-mean cloud feedback. In weakly ascending regions ($0 < \omega < -80$ hPa day^{-1}), the dynamic and nondynamic components are of similar magnitude but opposite signs. In descending regions, the nondynamic component controls the longwave feedback, while the shortwave feedback includes both dynamic and nondynamic contributions. Interestingly, feedbacks are almost entirely circulation-driven in regions of strong ascent ($\omega < -80$ hPa day^{-1}). The nonlinear component is small in all circulation regimes, but makes a statistically significant contribution in regions of weak ascent and descent.

The dynamic component reflects changes in CRE resulting from changes in the large-scale circulation: changing frequency of circulation regime occupancy drives CRE changes irrespective of changes in cloud properties. We find that, although the net dynamic feedback varies with vertical velocity (Fig. 3a), cancellation between positive feedbacks in regions of weak ascent and negative feedbacks elsewhere leads to a neutral tropical-mean influence: -0.13 ± 0.33 and -0.11 ± 0.37 W m^{-2} K^{-1} for DEEP-C and ERA5, respectively. Both the longwave and shortwave tropical-mean dynamic feedbacks are larger than the net dynamic feedback (e.g., -0.61 ± 0.36 and 0.48 ± 0.66 W m^{-2} K^{-1}, respectively, for DEEP-C, although only the longwave tropical-mean dynamic feedback is significantly nonzero). Figures 3b and 3c show the longwave and shortwave dynamic feedbacks as a function of vertical velocity. Because the climatological longwave and shortwave CRE(ω) relationships mirror each other (Fig. 1c), so do the dynamic feedbacks. However, the shortwave dynamic feedback dominates in all vertical velocity regimes because the magnitude of the climatological shortwave CRE is larger. Figures 4d–f show the spatial distribution of the DEEP-C dynamic component calculated following section 3b. The distribution can be understood through comparison to the spatial distribution of changes in vertical velocity (Fig. 2) and the climatological relationship between vertical velocity and CRE (Fig. 1c). Where ascent strengthens, we find strengthening CREs, and where ascent weakens, we find weakening CREs.

The nondynamic component of the cloud feedback reflects CRE changes driven by processes other than changes in $P(\omega)$. Because $P(\omega)$ peaks in regions of weak descent and ascent, these regions contribute most substantially to the nondynamic component of the cloud feedback. For DEEP-C, we find a neutral tropical-mean net nondynamic feedback of 0.28 ± 1.35 W m^{-2} K^{-1} resulting from compensating longwave and shortwave feedbacks of 2.15 ± 1.35 and -1.87 ± 1.36 W m^{-2} K^{-1}, respectively.

Although the longwave and shortwave nondynamic feedbacks both reflect strengthening CRE with increasing surface temperature, the spatial distribution of this strengthening is different. Consequently, net nondynamic feedbacks are positive in descending regions and negative in weakly ascending regions (Fig. 3). We turn to Figs. 4g–i to explore the spatial distribution of these trends further.

We find that nondynamic longwave and shortwave CRE strengthening is confined to oceanic regions, while over land, they generally weaken, especially in regions of ascent. Identifying the sources of nondynamic CRE changes is challenging given we do not have compatible datasets to estimate trends in cloud properties over the same time period. However, we hypothesize that in ascending regions over ocean, observed increases in surface temperature and specific humidity (Byrne and O'Gorman 2018) have led to increasing CRE via increasing cloud fraction and/or thickness. In contrast, observations show that the land relative humidity has declined over recent decades (Byrne and O'Gorman 2018; Simmons et al. 2021) which may have caused CRE reductions over continents (Kamae et al. 2016).

In regions of oceanic descent, the spatial pattern is more complex. Figure 4i shows that the nondynamic strengthening of shortwave CRE originates from regions of weak descent in the southern subtropical regions of the Pacific and Atlantic. Consequently, we suggest it is induced by warming west Pacific SSTs (Zhou et al. 2016). The warming SSTs lead to increased local

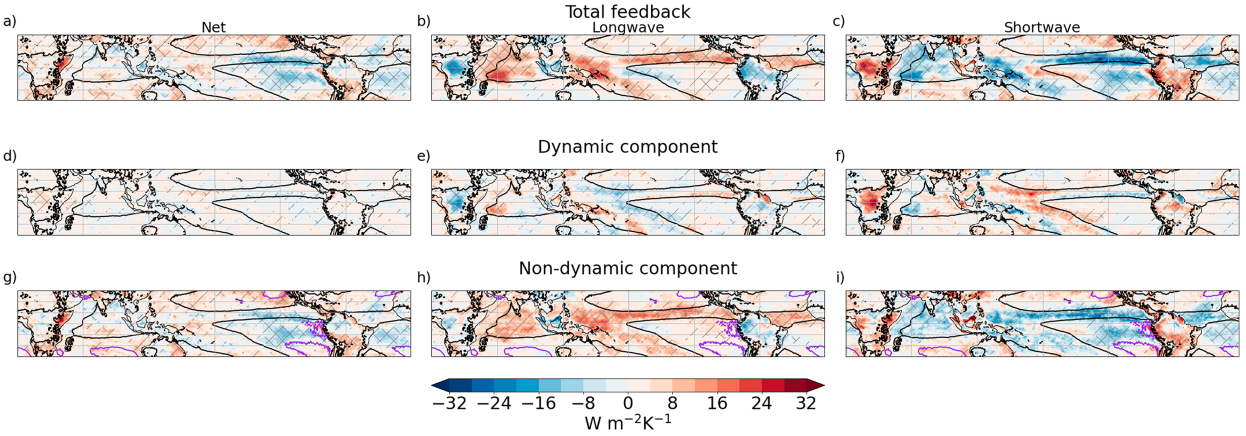

FIG. 4. DEEP-C estimates of the total (a) net, (b) longwave, and (c) shortwave cloud feedbacks calculated at each latitude and longitude. (d)–(f) The dynamic component and (g)–(i) the nondynamic component of the net, longwave, and shortwave cloud feedbacks, respectively, calculated following the method outlined in section 3b. Feedbacks are calculated from trends between 1985 and 2020. Regions where the magnitude of the feedback is larger than the standard error are hatched and regions where it is larger than twice the standard error are cross-hatched. The black contour divides regions of climatological ascent and descent. In (g)–(i), the purple contour shows oceanic regions in which $\omega > 25$ hPa day^{-1} more than 60% of the time.

convection which (due to weak temperature gradients in the tropical free troposphere) is able to increase the tropics-wide static stability and so strengthen the inversion in descending regions. This stability change combined with approximately constant local surface temperatures leads to increased low cloud [see section 4.2 of Sherwood et al. (2020) for further discussion of this mechanism]. If stability is indeed the controlling variable, this is an example of nonlocal circulation influences on CRE contributing to the nondynamic feedback.

In contrast, the spatial structure of the longwave nondynamic component in regions of weak descent is less clear (Fig. 4h), possibly indicating that the clouds contributing to this feedback are less spatially localized. There is some suggestion that strengthening longwave CRE occurs at the edges of ascending regions, and there is also strengthening in the east Pacific, collocated with the shortwave strengthening. Williams and Pierrehumbert (2017) show that high clouds, which largely control longwave feedbacks, can occur in both stable and marginally stable regimes, although most optically thick clouds occur in deep convective regimes. Thus, we hypothesize that the longwave feedbacks in descending regions are associated with high clouds which could be cirrus formed in situ, anvils which have been advected away from regions of climatological ascent, or, given our ω data are monthly means, high clouds resulting from occasional local convection.

The change in sign of the shortwave cloud feedbacks when transitioning from regions of weak to strong descent ($\omega > 25$ hPa day^{-1}) suggests that different mechanisms are at play once the local inversion strengthens (Fig. 1e). These regions include the stratocumulus decks west of Africa and South America (Figs. 4g–i, purple contours).

Comparing DEEP-C and ERA5, we find that the previously identified disagreement on shortwave feedbacks in the ~20-hPa vertical velocity regime leads to very different nondynamic feedbacks. Furthermore, scrutiny of the CRE time series in descending regions for DEEP-C (supplemental Fig. 3) reveals no obvious spurious short-term variability, for example, associated with the transition from ERBS WFOV to CERES during 1999–2000, which may influence the trends. Indeed, the ERA5 shortwave cloud feedback is more negative than the DEEP-C feedback over both the ERBS WFOV and CERES periods. We therefore hypothesize that the discrepancy between datasets may be associated with the challenge of capturing low-cloud feedbacks in the reanalysis given CRE is a modeled, rather than assimilated, variable. Additionally, we find that the spatial distribution of the discrepancies between the ERA5 and DEEP-C feedbacks (supplemental Fig. 4) mirrors the spatial distribution of discrepancies in the climatological CRE (supplemental Fig. 5), meaning if ERA5 feedbacks are indeed biased, this may result from biases in the mean state. The causes of these biases could be further investigated by comparing ERA5 cloud properties to observations.

The nonlinear component is a function of changes in both $P(\omega)$ and CRE(ω) [see (3)]. Although the nonlinear component is small for most circulation regimes, it is generally negative for longwave feedbacks and positive for shortwave feedbacks. This consistency leads to tropical-mean feedback values similar in magnitude to the dynamic component: -0.37 ± 0.07 W m^{-2} K^{-1}, 0.43 ± 0.09 W m^{-2} K^{-1}, and 0.06 ± 0.05 W m^{-2} K^{-1} for the DEEP-C longwave, shortwave, and net feedbacks, respectively.

d. Total cloud feedbacks

Figures 5a–c show the total contribution of each vertical velocity regime to the tropical-mean net, longwave, and shortwave cloud feedbacks, respectively (i.e., the sum of the dynamic, nondynamic, and nonlinear components). We find that dynamic feedbacks control the sign of longwave and shortwave feedbacks in ascending regions, while nondynamic feedbacks are more impactful in neutral and descending regions. We further find, within individual vertical velocity regimes, that longwave and shortwave feedbacks largely cancel. However, shortwave feedbacks

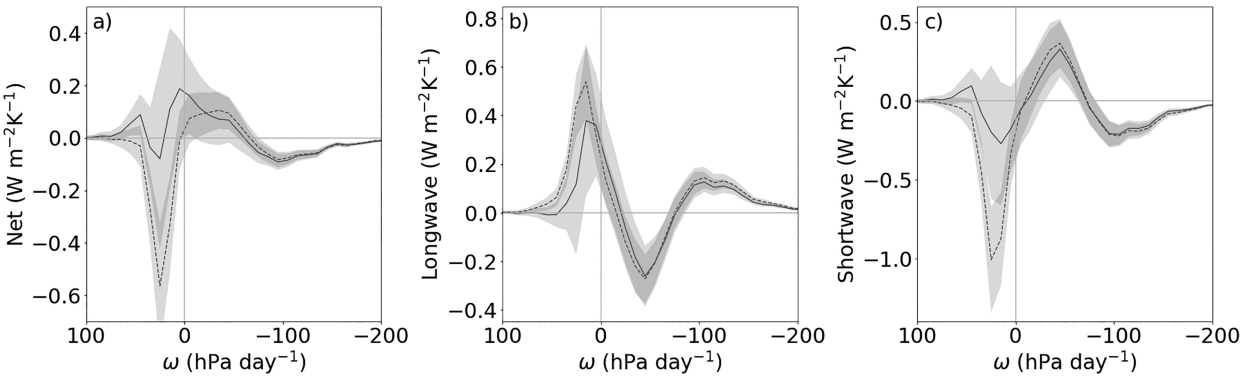

FIG. 5. DEEP-C (solid lines) and ERA5 (dashed lines) estimates of the contribution of each vertical velocity regime to the tropical-mean (a) net, (b) longwave, and (c) shortwave cloud feedbacks. Feedbacks are calculated from trends between 1985 and 2020. Shading shows twice the standard errors.

are stronger in all regimes except for regions of very weak descent, where positive longwave feedbacks dominate.

To calculate tropical-mean feedbacks, we sum over all vertical velocity regimes. Further cancellation between opposing shortwave feedbacks in different vertical velocity regimes leads to a neutral tropical-mean cloud feedback of 0.21 ± 1.39 W m^{-2} K^{-1}. Considering the tropical-mean longwave and shortwave feedbacks individually, we find that both reflect an overall strengthening of CRE over the period 1985–2020, with values of 1.17 ± 1.40 and -0.96 ± 1.52 W m^{-2} K^{-1}, respectively, although the shortwave change is not significant at the 95% confidence interval. As expected, ERA5 estimates of the tropical-mean feedback differ substantially from DEEP-C estimates, with ERA5 showing a negative tropical-mean net cloud feedback of -1.30 ± 0.42 W m^{-2} K^{-1} and longwave and shortwave tropical-mean feedbacks of 1.87 ± 0.38 and -3.17 ± 0.72 W m^{-2} K^{-1}, respectively. We note that, due to the inclusion of instrument error, the DEEP-C tropical-mean feedback estimates have larger errors than the ERA5 estimates and previous observational estimates. However, we believe these estimates remain valuable given they are based on trends, rather than variability, and use a previously unexplored multidecadal dataset.

Supplemental Table 1 compares these results to estimates calculated using trends in tropical-mean CRE anomalies. We find that, although the feedback estimates are not identical, they agree closely and the net and shortwave feedbacks agree within regression error. Differences may arise for a range of reasons, but we highlight that we do not incorporate the standard errors on the tropical-mean or vertical velocity regime-mean CREs or on the surface temperature mean into the regressions.

5. Implications for interpreting cloud feedbacks

a. Small tropical-mean dynamic component

Despite recent decades displaying significant trends in the tropical (Fig. 1b) and large circulation-driven cloud feedbacks across a range of vertical velocity regimes (Fig. 3a), we find that, when averaged over the tropics, the dynamic components of both the longwave and shortwave cloud feedbacks are small compared to the nondynamic components (section 4c). Furthermore, the tropical-mean net dynamic feedback is not significantly nonzero for DEEP-C or ERA5 (section 4c). To interpret these results, we consider mass budget constraints on the dynamic feedback. Following Wyant et al. (2006) and Byrne and Schneider (2018), we explore the implications for the dynamic feedbacks of a linear relationship between CRE and vertical velocity. Assuming $\mathrm{CRE}(\omega, m) = a(m) + b(m)\omega$, where a and b are the arbitrary constants, and substituting this linear relationship into the expression for the dynamic component, we find

$$\sum_{\omega}\left\langle \mathrm{CRE}(\omega, m)\frac{dP(\omega, m, y)}{d\overline{T}(m, y)}\right\rangle = \sum_{\omega}\left\langle a(m)\frac{dP(\omega, m, y)}{d\overline{T}(m, y)} + b(m)\omega\frac{dP(\omega, m, y)}{d\overline{T}(m, y)}\right\rangle. \quad (8)$$

By construction, the integral of $dP(\omega, m, y)/d\overline{T}(m, y)$ over all vertical velocity regimes is zero for each month. The global integral of $\omega dP(\omega, m, y)/d\overline{T}(m, y)$ is also expected to be zero for each month, as maintaining constant atmospheric mass requires equal trends in upward and downward mass fluxes. Thus, the global-mean dynamic component, in the limit of linear $\mathrm{CRE}(\omega, m)$ relationships, is zero. The tropics is not a closed mass system, so the mass flux requirement does not necessarily hold in this study. However, evaluating the integral of $\omega dP(\omega, m, y)/d\overline{T}(m, y)$ results in an area-weighted vertical velocity trend of -0.20 ± 0.24 hPa day^{-1} K^{-1}, i.e., no significant trend.

Now we know that this framework can be approximately applied to interpret our results, we turn to the observed climatological relationship between CRE and ω (Fig. 1c). As discussed in section 4b, we find that the longwave and shortwave $\mathrm{CRE}(\omega)$ relationships exhibit substantial nonlinearity. In descending regions, the curves plateau, and in ascending regions, the curve is approximately quadratic, with weakening longwave and shortwave CREs as ω decreases beyond ~ -100 hPa day^{-1}. Interestingly, these observational estimates of $\mathrm{CRE}(\omega)$ contradict the quasi-linear relationships found for the multimodel mean of CMIP5 models (Byrne and Schneider 2018). Rather, the relationships align more closely with results from cloud-

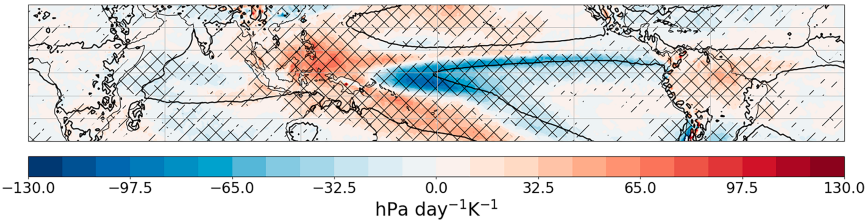

FIG. 6. Changes in vertical velocity per degree tropical warming calculated from detrended interannual variability between 1985 and 2020. Regions where the magnitude of the sensitivity to warming is larger than the standard error are hatched and regions where it is larger than twice the standard error are cross-hatched. The black contour divides regions of climatological ascent and descent.

resolving models (Mackie and Byrne 2023) although, in the multimodel mean, these models do not show a decline in CRE magnitude beyond ~ -100 hPa day^{-1}. Similar behavior in regions of strong ascent can be found in earlier analyses of satellite data (Bony et al. 2004; Wyant et al. 2006). Recent work also finds substantial nonlinearity in CRE(ω) estimated from CERES-EBAF data, with implications for GCM estimates of dynamic feedbacks (Hill et al. 2023). However, we find that the nonlinearity produces only modest longwave and shortwave tropical-mean dynamic feedbacks. This is because the magnitude of the dynamic component depends on the location in ω space of nonlinearities in the CRE(ω) functions relative to the circulation changes (Mackie and Byrne 2023; Hill et al. 2023).

The nonlinearity of the relationship between net CRE and ω is determined by the relative shapes of the longwave and shortwave CRE(ω) relationships. As the nonlinearities in these relationships are mirrored, the net CRE(ω) curve is quasi-linear (Fig. 1c), leading to a neutral net dynamic feedback. Because the neutrality of this feedback is a consequence of the climatological relationship between net CRE and ω, we suggest that this finding is approximately independent of the nature of the circulation change. However, an important caveat to this conclusion is that we do not use observed vertical velocities (and these are not directly assimilated in the reanalysis), meaning net CRE(ω) could be more nonlinear in reality. A secondary caveat is that imperfections in the linearity of our CRE(ω) curve imply that a larger dynamic component in the future is plausible; however, this would require future circulation changes to differ substantially (in ω space) from recent trends.

The constraints imposed by the atmospheric mass budget on circulation-driven changes in clouds and CRE have implications for how we analyze and interpret cloud feedbacks. As shown in Fig. 3, the negligible tropical-mean dynamic component results from the cancellation of large dynamic feedbacks in different vertical velocity regimes. This means that current estimates of feedbacks associated with individual cloud types (e.g., Sherwood et al. 2020) likely include substantial dynamic components. However, when area averaged, these dynamic components are expected to approximately cancel, so it may be useful to isolate the *nondynamic components* when estimating feedbacks for individual cloud types. It is these nondynamic components that are expected to dominate cloud feedbacks on the large scales relevant for climate sensitivity estimates, for example, but which are often conflated with dynamic components in traditional feedback decompositions. Focusing on the nondynamic components of feedbacks associated with individual cloud regimes may provide new insights into the relative magnitudes of both the feedbacks themselves and the uncertainties in their estimates.

b. *Estimating feedbacks using trends versus variability*

Due to the limited timespan of satellite datasets, observational estimates of cloud feedbacks have previously focused on short-term covariability between temperature and CRE (e.g., Dessler and Loeb 2013). However, the extent to which cloud feedbacks estimated using short-term variability are representative of long-term, anthropogenically forced cloud feedbacks is an open question. To gain insight into this question, we repeat our analysis using detrended short-term variability rather than multidecadal trends.

The substantial contribution of the dynamic component to trend-derived cloud feedbacks within individual vertical velocity regimes (Fig. 3) suggests that, for variability-derived feedbacks to resemble these results, the sensitivities of circulation to tropical-mean temperature variability and trends must be similar. Comparison of Figs. 2 and 6, which show changes in vertical velocity per degree tropical-mean warming derived from trends and from detrended interannual variability, respectively, indicates that this is not the case. Interannual circulation sensitivity in the tropics is dominated by ENSO, but the pattern of long-term circulation sensitivity is distinct. In vertical velocity space, the circulation sensitivities have similar shapes (Fig. 7a vs Fig. 1b), but the magnitude of the variability-derived circulation sensitivity is substantially smaller across regimes. Furthermore, the variability-derived case does not reproduce the reduction in the frequency of very weak ascent ($-30 < \omega < 0$ hPa day^{-1}) or the increase in the frequency of very strong ascent ($\omega < -80$ hPa day^{-1}) seen in the trend-derived case. Note that, as expected given the conclusions of section 5a, the variability derived tropics-wide dynamic component is of a similar magnitude to the trend-derived estimate and is not significantly nonzero (e.g., 0.16 ± 0.30 W m^{-2} K^{-1} for DEEP-C).

Figures 7b and 7c show the variability-derived cloud feedbacks that are not associated with changes in the vertical

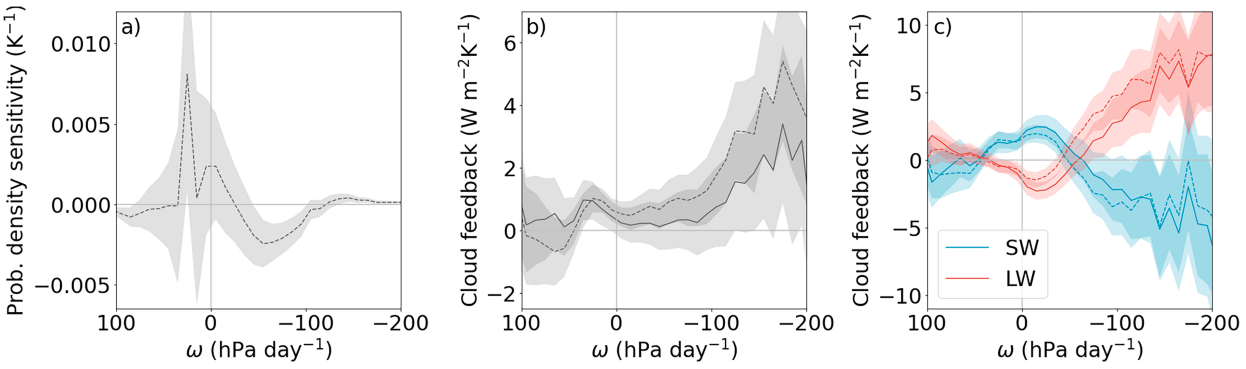

FIG. 7. DEEP-C (solid lines) and ERA5 (dashed lines) estimates of (a) the probability density sensitivity $dP(\omega)/d\overline{T}$ and the (b) net and (c) longwave and shortwave cloud feedbacks $d\mathrm{CRE}(\omega)/d\overline{T}$. Feedbacks are calculated from detrended interannual variability between 1985 and 2020. Shading shows twice the standard errors.

velocity distribution. Comparison to the trend-derived feedbacks (Figs. 1d,e) shows that these also differ substantially, meaning it is not just the circulation sensitivities which differ on the two time scales. In fact, the trend-derived and variability-derived nondynamic feedbacks differ in sign in many vertical velocity regimes for both the longwave and shortwave feedbacks. We hypothesize that an important contribution to the dissimilarity could be the thermodynamic impact of different surface warming patterns associated with trends versus interannual variability.

In conclusion, we find that both the dynamic and the nondynamic mechanisms through which clouds respond to surface temperature changes are different for trends versus variability. This suggests a nuanced approach is needed when estimating cloud feedbacks from variability. An example of this is the use of cloud-controlling factors (CCFs) (Klein et al. 2018; Ceppi and Nowack 2021; Myers et al. 2021; Datseris et al. 2022). In this framework, the response of CRE to a change in mean surface temperature is mediated by the responses of a set of other variables, or CCFs. The relationship between changes in CCFs and changes in CRE are assumed to be independent of the temporal scale considered because clouds typically respond to their surroundings on subdaily time scales. However, the relationship between CCFs and mean surface temperature must be calculated over the time period of interest.

c. *Estimation of the combined tropical anvil area and albedo feedback*

The response of tropical anvil area and albedo to warming are leading sources of uncertainty in estimates of the total cloud feedback and the climate sensitivity. As discussed in Sherwood et al. (2020), GCMs and cloud-resolving models likely provide poor estimates of these feedbacks due to challenges in parameterizing subgrid-scale processes. Consequently, observations constitute an important data source for investigating these feedbacks. Sherwood et al. (2020) assess likely values of the combined anvil area and albedo feedback (which they call the "tropical anvil cloud area feedback") using a study by Williams and Pierrehumbert (2017) of observed year-to-year covariability of CRE and surface temperature in the tropics. Here, we use understanding developed in earlier sections of this work to expand on the results of Williams and Pierrehumbert (2017) and provide new estimates of this important feedback. To do this, we make use of the DEEP-C dataset, i.e., DEEP-C all-sky fluxes combined with ERA5 clear-sky fluxes and vertical velocities.

First, we estimate the tropical anvil area feedback using observed trends rather than variability. We use the same method as previously, except the analysis is performed over tropical oceans only and the global mean (rather than tropical-mean) temperature time series is used for consistency with Sherwood et al. (2020). Additionally, we only integrate over vertical velocity regimes with $\omega < 0$ hPa day^{-1} to isolate the contribution of ascending regions. We then remove the cloud altitude feedback to convert to a feedback associated only with area and albedo changes. Following Sherwood et al. (2020), we use their Fig. 5d to estimate the cloud altitude feedback local to regions of oceanic ascent as $+0.40$ W m^{-2} K^{-1} and then scale this value by the ratio of the area of ascent over tropical oceans to the total tropical ocean area (S. Klein 2023, personal communication). Finally, we use a further area scaling to convert from a tropical-ocean-wide feedback to a global-mean feedback. A more detailed description of the calculation can be found in the supplemental material.

We obtain a negative global anvil area and albedo feedback of -0.30 ± 0.16 W m^{-2} K^{-1}, suggesting changes in these cloud properties have had a robust stabilizing influence on TOA radiative fluxes over recent decades. In contrast, variability-derived estimates do not exclude a weak feedback. Repeating the calculation for detrended interannual variability gives a feedback of -0.14 ± 0.11 W m^{-2} K^{-1}. Note also that the trend-derived feedback estimate lies outside of the 2σ error range of the variability-derived estimate. Previous variability-derived estimates of the global anvil area and albedo feedback by Sherwood et al. (2020) and Chao et al. (2024) are -0.20 ± 0.20 (1σ) and 0.01 ± 0.05 W m^{-2} K^{-1} (90% confidence level), respectively. There are likely multiple contributors to the different variability-derived feedback estimates. For example, differences may arise due to the time period considered, the observational dataset used, and whether the data are detrended.

Furthermore, Chao et al. (2024) used a substantially different method, focusing their analysis on high clouds and using CERES Flux by Cloud Type (CERES-FBCT) and MODIS-COSP data combined with cloud radiative kernels to quantify the sensitivity of TOA radiation to cloud-top pressure and cloud visible optical depth.

Second, we estimate the tropical anvil area feedback using only the nondynamic component of the trend-derived feedback, given our results suggest that, tropics-wide, dynamic feedbacks largely cancel. In this case, we obtain a feedback of -0.28 ± 0.14 W m^{-2} K^{-1}. Cancellation of the longwave and shortwave dynamic feedbacks in ascending regions means that the magnitude of the net tropical anvil area feedback is only slightly impacted by the change in methodology; however, the error on the result is reduced by 8%.

We note that the assumption that anvil clouds control feedbacks in regions of climatological ascent is a simplification. Changes in CREs in ascending regions are not exclusively associated with anvils and anvils may be advected into regions of monthly mean descent over the course of their lifetime.

Because the CRE of tropical anvils varies over their lifetime (Hartmann et al. 2018), our feedback estimate could be more influenced by CRE changes in convective cores than during later stages of the anvil lifetime. Indeed, Sokol et al. (2024) find a neutral anvil feedback resulting from cancellation between a negative feedback in the cores and a positive feedback in the remainder of the anvil. Raghuraman et al. (2024) estimated short-term area and albedo feedbacks for high clouds over the entire tropics (comprising tropical anvils and in situ cirrus) using CERES-FBCT. They find an area feedback of -0.03 ± 0.03 W m^{-2} K^{-1} and an albedo feedback of 0.03 ± 0.05 W m^{-2} K^{-1}, again suggesting that focusing on regions of climatological ascent may exclude a positive feedback component from regions of climatological descent.

A further caveat to these results is that the estimate we use for the cloud altitude feedback is obtained from the response of GCMs to an abrupt 4xCO_2 forcing. Aside from potential problems with the models themselves, this feedback is estimated from a radiative forcing that is different to that acting over the time period considered here.

6. Summary and discussion

Tropical cloud feedbacks remain a key source of uncertainty in estimates of equilibrium climate sensitivity (Sherwood et al. 2020). This study leverages the DEEP-C all-sky radiative flux dataset and combines it with ERA5 clear-sky fluxes to explore the processes driving the tropical cloud feedbacks associated with multidecadal trends in CRE and tropical-mean surface temperature. Isolation of the circulation-driven component of the feedback following Bony et al. (2004) allows insight into the role of interactions between clouds and the large-scale atmospheric circulation on CRE changes.

We find that circulation changes induce substantial tropical cloud feedbacks. For a given vertical velocity regime, the magnitudes of the dynamic and nondynamic feedback components are comparable, and in regions of strong ascent, the feedbacks are almost entirely dynamically driven (Fig. 3). The origin of the dynamic component is primarily a narrowing and strengthening of regions of tropical ascent. However, while circulation-driven feedbacks play an important role in determining regional cloud feedbacks, their contribution to the tropical-mean net cloud feedback is small and not significantly different from zero. The dynamic feedback is constrained by the atmospheric mass budget which, combined with the approximately linear relationship between net CRE and vertical velocity, limits the contribution of circulation changes to cloud feedbacks on large scales. Because this limitation is independent of the nature of the circulation change, it is likely that the dynamic component will remain small as the anthropogenically forced climate change signal emerges. We suggest that focusing on the nondynamic components of individual cloud feedbacks may provide new perspectives on the relative magnitudes of these feedbacks, their errors, and their influence on climate sensitivity.

Nondynamically driven changes dominate the tropical-mean cloud feedback. Exploring the spatial distribution of these changes, we find that, over land, CREs weaken. If, as we hypothesize, this is driven by decreasing relative humidity over land, this may continue with increasing CO_2 forcing (Byrne and O'Gorman 2016). In regions of climatological ascent over ocean, CREs strengthen. Here, we hypothesize that this is due to increasing humidity and surface temperature which, again, is likely to continue in future (Held and Soden 2006). In regions of climatological descent over ocean, we find strengthening shortwave CRE, likely a result of increasing west Pacific SSTs leading to increased local ascent, tropics-wide static stability, and low cloud amount (Zhou et al. 2016). GCMs suggest CO_2 forcing will reduce the east–west SST gradient and decrease low cloud; however, Wills et al. (2022) show these models are largely unable to capture the observed trend. Chao et al. (2022) highlight that the pattern of Pacific SSTs is of fundamental importance to the global-mean cloud feedback.

We also show that both dynamic and nondynamic cloud feedbacks estimated using short-term covariability between CRE and tropical-mean surface temperature differ substantially from those estimated using trends (Figs. 1, 7), suggesting variability-derived feedback estimates should be interpreted with caution. The dynamic component of the feedback differs because the circulation change mechanisms are different on the two time scales: Unlike multidecadal trends, circulation variability is dominated by ENSO. As past estimates of the uncertain and influential anvil area and albedo feedbacks have relied on variability, we follow Williams and Pierrehumbert (2017) and Sherwood et al. (2020) to produce new trend-derived estimates of the total and nondynamic component of this feedback (-0.30 ± 0.16 and -0.28 ± 0.14 W m^{-2} K^{-1}, respectively).

Integrating over all vertical velocity regimes yields estimates of tropical-mean cloud feedbacks. For the period 1985–2020, we obtain a neutral net cloud feedback of 0.21 ± 1.39 W m^{-2} K^{-1}. This neutral feedback appears to result from cancellation between strengthening longwave and shortwave feedbacks (1.17 ± 1.40 and -0.96 ± 1.52, respectively) but large errors, primarily associated with gaps in the DEEP-C record, render these results inconclusive.

The feedback estimates presented in this study have several limitations. Importantly, the extent to which the estimates are representative of CO_2-forced changes is unclear, given the confounding influences of aerosol forcing and natural variability. This is exemplified by the differences in trend-derived feedback estimates calculated over the CERES (2000–20) versus DEEP-C (1985–2020) periods (supplemental Table 2). Furthermore, we do not separate the surface temperature–mediated cloud feedbacks from rapid cloud adjustments. Raghuraman et al. (2023) showed that the contribution from cloud adjustments to recent CRE trends is substantial. Although their method relies on model estimates for this adjustment, thus potentially introducing errors, it presents an interesting avenue for further exploration of the DEEP-C dataset. We also note that we use relatively simple tools to explore the trends in the data. Consideration of the impact of regression method, start and end dates, and the degree of autocorrelation in the time series would add to the reliability of the results. More broadly, we suggest that the sensitivity of trend-derived feedback estimates to methodological and dataset choices should be systematically explored, particularly given the short period over which we have observations. To our knowledge, observed clear-sky radiative fluxes are not available for the DEEP-C time period; however, we note that the use of CERES-EBAF versus ERA5 clear-sky fluxes influences longwave feedback estimates (supplemental Table 2).

This study presents a number of avenues for future work. First, we identify several interesting questions: What controls the climatological relationship between the longwave and shortwave CREs and ω? And why is the climatological net CRE relatively insensitive to vertical velocity? Second, while the simple decomposition of Bony et al. (2004) provides new physical insight into observed cloud feedbacks, it cannot fully characterize the complex connections between CRE and atmospheric circulation. Can the decomposition be extended to capture the effects of spatial shifts in circulation on cloud feedbacks? Or to explore how circulation changes couple to remote cloud feedbacks? Finally, the relationships between clouds and circulation presented here provide a useful observational benchmark against which GCMs and the emerging global storm-resolving models can be compared.

Acknowledgments. E. V. thanks Anna Mackie, Richard P. Allan, Stephen A. Klein, Ryan J. Kramer, and Ian N. Williams for helpful discussions. We additionally thank the reviewers for their thoughtful feedback. E. V. acknowledges funding from the U.K. Natural Environment Research Council, Doctoral Training Partnership in Environmental Research (Grant NE/S007474/1). M. P. B. was supported by the U.K. Natural Environment Research Council (Grant NE/T006269/1). This work used JASMIN, the U.K. collaborative data analysis facility.

Data availability statement. Previously published datasets were used for this work and are all publicly available. DEEP-C data can be accessed at https://doi.org/10.17864/1947.000347 and ERA5 data were obtained from the Copernicus Climate Data Store and are available at https://doi.org/10.24381/cds.6860a573 (variables on pressure levels) and https://doi.org/10.24381/cds.f17050d7 (variables on single levels). Radiative kernels can be downloaded from the University of Miami Radiative Kernel Portal (https://climate.earth.miami.edu/data/radiative-kernels/).

REFERENCES

Allan, R. P., C. Liu, N. G. Loeb, M. D. Palmer, M. Roberts, D. Smith, and P.-L. Vidale, 2014: Changes in global net radiative imbalance 1985–2012. *Geophys. Res. Lett.*, **41**, 5588–5597, https://doi.org/10.1002/2014GL060962.

Bloch-Johnson, J., and Coauthors, 2024: The Green's Function Model Intercomparison Project (GFMIP) protocol. *J. Adv. Model. Earth Syst.*, **16**, e2023MS003700, https://doi.org/10.1029/2023MS003700.

Bony, S., J.-L. Dufresne, H. L. Treut, J.-J. Morcrette, and C. Senior, 2004: On dynamic and thermodynamic components of cloud changes. *Climate Dyn.*, **22**, 71–86, https://doi.org/10.1007/s00382-003-0369-6.

——, and Coauthors, 2015: Clouds, circulation and climate sensitivity. *Nat. Geosci.*, **8**, 261–268, https://doi.org/10.1038/ngeo2398.

Byrne, M. P., and P. A. O'Gorman, 2016: Understanding decreases in land relative humidity with global warming: Conceptual model and GCM simulations. *J. Climate*, **29**, 9045–9061, https://doi.org/10.1175/JCLI-D-16-0351.1.

——, and ——, 2018: Trends in continental temperature and humidity directly linked to ocean warming. *Proc. Natl. Acad. Sci. USA*, **115**, 4863–4868, https://doi.org/10.1073/pnas.1722312115.

——, and T. Schneider, 2018: Atmospheric dynamics feedback: Concept, simulations, and climate implications. *J. Climate*, **31**, 3249–3264, https://doi.org/10.1175/JCLI-D-17-0470.1.

——, A. G. Pendergrass, A. D. Rapp, and K. R. Wodzicki, 2018: Response of the intertropical convergence zone to climate change: Location, width, and strength. *Curr. Climate Change Rep.*, **4**, 355–370, https://doi.org/10.1007/s40641-018-0110-5.

Ceppi, P., and P. Nowack, 2021: Observational evidence that cloud feedback amplifies global warming. *Proc. Natl. Acad. Sci.*, **118**, e2026290118, https://doi.org/10.1073/pnas.2026290118.

Chao, L.-W., J. C. Muller, and A. E. Dessler, 2022: Impacts of the unforced pattern effect on the cloud feedback in CERES observations and climate models. *Geophys. Res. Lett.*, **49**, e2021GL096299, https://doi.org/10.1029/2021GL096299.

——, M. D. Zelinka, and A. E. Dessler, 2024: Evaluating cloud feedback components in observations and their representation in climate models. *J. Geophys. Res. Atmos.*, **129**, e2023JD039427, https://doi.org/10.1029/2023JD039427.

Datseris, G., J. Blanco, O. Hadas, S. Bony, R. Caballero, Y. Kaspi, and B. Stevens, 2022: Minimal recipes for global cloudiness. *Geophys. Res. Lett.*, **49**, e2022GL099678, https://doi.org/10.1029/2022GL099678.

Dessler, A. E., 2010: A determination of the cloud feedback from climate variations over the past decade. *Science*, **330**, 1523–1527, https://doi.org/10.1126/science.1192546.

——, and N. G. Loeb, 2013: Impact of dataset choice on calculations of the short-term cloud feedback. *J. Geophys. Res. Atmos.*, **118**, 2821–2826, https://doi.org/10.1002/jgrd.50199.

Feldl, N., and G. H. Roe, 2013: Four perspectives on climate feedbacks. *Geophys. Res. Lett.*, **40**, 4007–4011, https://doi.org/10.1002/grl.50711.

Hartmann, D. L., B. Gasparini, S. E. Berry, and P. N. Blossey, 2018: The life cycle and net radiative effect of tropical anvil clouds. *J. Adv. Model. Earth Syst.*, **10**, 3012–3029, https://doi.org/10.1029/2018MS001484.

Held, I. M., and B. J. Soden, 2006: Robust responses of the hydrological cycle to global warming. *J. Climate*, **19**, 5686–5699, https://doi.org/10.1175/JCLI3990.1.

Hersbach, H., and Coauthors, 2020: The ERA5 global reanalysis. *Quart. J. Roy. Meteor. Soc.*, **146**, 1999–2049, https://doi.org/10.1002/qj.3803.

Hill, P. G., C. E. Holloway, M. P. Byrne, F. H. Lambert, and M. J. Webb, 2023: Climate models underestimate dynamic cloud feedbacks in the tropics. *Geophys. Res. Lett.*, **50**, e2023GL104573, https://doi.org/10.1029/2023GL104573.

Hollmann, R., and S. Pinnock, 2020: ESA Cloud_cci Product Validation and Intercomparison Report (PVIR). European Space Agency Tech. Rep., 159 pp., https://climate.esa.int/media/documents/Cloud_Product-Validation-and-Intercomparison-Report-PVIR_v6.0.pdf.

Kamae, Y., T. Ogura, M. Watanabe, S.-P. Xie, and H. Ueda, 2016: Robust cloud feedback over tropical land in a warming climate. *J. Geophys. Res. Atmos.*, **121**, 2593–2609, https://doi.org/10.1002/2015JD024525.

Klein, S. A., A. Hall, J. R. Norris, and R. Pincus, 2018: Low-cloud feedbacks from cloud-controlling factors: A review. *Shallow Clouds, Water Vapor, Circulation, and Climate Sensitivity*, R. Pincus, D. Winker, S. Bony, and B. Stevens, Eds., Space Sciences Series of ISSI, Vol. 65, Springer, 135–157.

Kramer, R. J., A. V. Matus, B. J. Soden, and T. S. L'Ecuyer, 2019: Observation-based radiative kernels from CloudSat/CALIPSO. *J. Geophys. Res. Atmos.*, **124**, 5431–5444, https://doi.org/10.1029/2018JD029021.

Liu, C., and R. Allan, 2022: Reconstructions of the radiation fluxes at the top of atmosphere and net surface energy flux: DEEP-C version 5.0. University of Reading, accessed 12 August 2021, https://researchdata.reading.ac.uk/347/.

——, and Coauthors, 2015: Combining satellite observations and reanalysis energy transports to estimate global net surface energy fluxes 1985–2012. *J. Geophys. Res. Atmos.*, **120**, 9374–9389, https://doi.org/10.1002/2015JD023264.

——, and Coauthors, 2020: Variability in the global energy budget and transports 1985–2017. *Climate Dyn.*, **55**, 3381–3396, https://doi.org/10.1007/s00382-020-05451-8.

Loeb, N. G., and Coauthors, 2018: Clouds and the Earth's Radiant Energy System (CERES) Energy Balanced And Filled (EBAF) top-of-atmosphere (TOA) edition-4.0 data product. *J. Climate*, **31**, 895–918, https://doi.org/10.1175/JCLI-D-17-0208.1.

Ma, S., and T. Zhou, 2016: Robust strengthening and westward shift of the tropical Pacific Walker circulation during 1979–2012: A comparison of 7 sets of reanalysis data and 26 CMIP5 models. *J. Climate*, **29**, 3097–3118, https://doi.org/10.1175/JCLI-D-15-0398.1.

Mackie, A., and M. P. Byrne, 2023: Effects of circulation on tropical cloud feedbacks in high-resolution simulations. *J. Adv. Model. Earth Syst.*, **15**, e2022MS003516, https://doi.org/10.1029/2022MS003516.

McKim, B., S. Bony, and J.-L. Dufresne, 2024: Weak anvil cloud area feedback suggested by physical and observational constraints. *Nat. Geosci.*, **17**, 392–397, https://doi.org/10.1038/s41561-024-01414-4.

Myers, T. A., R. C. Scott, M. D. Zelinka, S. A. Klein, J. R. Norris, and P. M. Caldwell, 2021: Observational constraints on low cloud feedback reduce uncertainty of climate sensitivity. *Nat. Climate Change*, **11**, 501–507, https://doi.org/10.1038/s41558-021-01039-0.

Norris, J. R., and A. T. Evan, 2015: Empirical removal of artifacts from the ISCCP and PATMOS-x satellite cloud records. *J. Atmos. Oceanic Technol.*, **32**, 691–702, https://doi.org/10.1175/JTECH-D-14-00058.1.

Raghuraman, S. P., D. Paynter, and V. Ramaswamy, 2021: Anthropogenic forcing and response yield observed positive trend in Earth's energy imbalance. *Nat. Commun.*, **12**, 4577, https://doi.org/10.1038/s41467-021-24544-4.

——, ——, R. Menzel, and V. Ramaswamy, 2023: Forcing, cloud feedbacks, cloud masking, and internal variability in the cloud radiative effect satellite record. *J. Climate*, **36**, 4151–4167, https://doi.org/10.1175/JCLI-D-22-0555.1.

——, B. Medeiros, and A. Gettelman, 2024: Observational quantification of tropical high cloud changes and feedbacks. *J. Geophys. Res. Atmos.*, **129**, e2023JD039364, https://doi.org/10.1029/2023JD039364.

Shell, K. M., J. T. Kiehl, and C. A. Shields, 2008: Using the radiative kernel technique to calculate climate feedbacks in NCAR's Community Atmospheric Model. *J. Climate*, **21**, 2269–2282, https://doi.org/10.1175/2007JCLI2044.1.

Sherwood, S. C., and Coauthors, 2020: An assessment of Earth's climate sensitivity using multiple lines of evidence. *Rev. Geophys.*, **58**, e2019RG000678, https://doi.org/10.1029/2019RG000678.

Simmons, A., and Coauthors, 2021: Low frequency variability and trends in surface air temperature and humidity from ERA5 and other datasets. ECMWF Tech. Memo. 881, 99 pp., https://doi.org/10.21957/ly5vbtbfd.

Sokol, A. B., C. J. Wall, and D. L. Hartmann, 2024: Greater climate sensitivity implied by anvil cloud thinning. *Nat. Geosci.*, **17**, 398–403, https://doi.org/10.1038/s41561-024-01420-6.

Stengel, M., and Coauthors, 2020: Cloud_cci Advanced Very High Resolution Radiometer Post Meridiem (AVHRR-PM) dataset version 3: 35-year climatology of global cloud and radiation properties. *Earth Syst. Sci. Data*, **12**, 41–60, https://doi.org/10.5194/essd-12-41-2020.

Su, H., L. Wu, C. Zhai, J. H. Jiang, J. D. Neelin, and Y. L. Yung, 2020: Observed tightening of tropical ascent in recent decades and linkage to regional precipitation changes. *Geophys. Res. Lett.*, **47**, e2019GL085809, https://doi.org/10.1029/2019GL085809.

Wall, C. J., J. R. Norris, A. Possner, D. T. McCoy, I. L. McCoy, and N. J. Lutsko, 2022: Assessing effective radiative forcing from aerosol–cloud interactions over the global ocean. *Proc. Natl. Acad. Sci.*, **119**, e2210481119, https://doi.org/10.1073/pnas.2210481119.

Wielicki, B. A., and Coauthors, 2002: Evidence for large decadal variability in the tropical mean radiative energy budget. *Science*, **295**, 841–844, https://doi.org/10.1126/science.1065837.

Williams, I. N., and R. T. Pierrehumbert, 2017: Observational evidence against strongly stabilizing tropical cloud feedbacks. *Geophys. Res. Lett.*, **44**, 1503–1510, https://doi.org/10.1002/2016GL072202.

Wills, R. C. J., Y. Dong, C. Proistosecu, K. C. Armour, and D. S. Battisti, 2022: Systematic climate model biases in the large-scale patterns of recent sea-surface temperature and sea-level pressure change. *Geophys. Res. Lett.*, **49**, e2022GL100011, https://doi.org/10.1029/2022GL100011.

Wodzicki, K. R., and A. D. Rapp, 2016: Long-term characterization of the Pacific ITCZ using TRMM, GPCP, and ERA-

Interim. *J. Geophys. Res. Atmos.*, **121**, 3153–3170, https://doi.org/10.1002/2015JD024458.

Wong, T., B. A. Wielicki, R. B. Lee III, G. L. Smith, K. A. Bush, and J. K. Willis, 2006: Reexamination of the observed decadal variability of the Earth radiation budget using altitude-corrected ERBE/ERBS nonscanner WFOV data. *J. Climate*, **19**, 4028–4040, https://doi.org/10.1175/JCLI3838.1.

Wyant, M. C., C. S. Bretherton, J. T. Bacmeister, J. T. Kiehl, I. M. Held, M. Zhao, S. A. Klein, and B. J. Soden, 2006: A comparison of low-latitude cloud properties and their response to climate change in three AGCMs sorted into regimes using mid-tropospheric vertical velocity. *Climate Dyn.*, **27**, 261–279, https://doi.org/10.1007/s00382-006-0138-4.

Young, A. H., K. R. Knapp, A. Inamdar, W. Hankins, and W. B. Rossow, 2018: The International Satellite Cloud Climatology Project H-series climate data record product. *Earth Syst. Sci. Data*, **10**, 583–593, https://doi.org/10.5194/essd-10-583-2018.

Zelinka, M. D., T. A. Myers, D. T. McCoy, S. Po-Chedley, P. M. Caldwell, P. Ceppi, S. A. Klein, and K. E. Taylor, 2020: Causes of higher climate sensitivity in CMIP6 models. *Geophys. Res. Lett.*, **47**, e2019GL085782, https://doi.org/10.1029/2019GL085782.

Zhou, C., M. D. Zelinka, and S. A. Klein, 2016: Impact of decadal cloud variations on the Earth's energy budget. *Nat. Geosci.*, **9**, 871–874, https://doi.org/10.1038/ngeo2828.